

# Thermal smart materials with tunable thermal conductivity: Mechanisms, materials, and applications

ZiTong Zhang, and BingYang Cao\*

*Key Laboratory for Thermal Science and Power Engineering of Ministry of Education, Department of Engineering Mechanics,  
Tsinghua University, Beijing 100084, China*

Received February 28, 2022; accepted May 7, 2022; published online September 30, 2022

The demand for active and effective management of heat transfer is increasing in various modern application scenarios. The thermal conductivity of materials plays a key role in thermal management systems, and reversibly tunable thermal properties are one of the fundamental needs for materials. Thermal smart materials, whose thermal properties can be tuned with an external trigger, have attracted the attention of researchers. In this paper, we provide a brief review of current research advances in thermal smart materials in recent years in terms of fundamental physical mechanisms, thermal switching ratios, and their application value. We focus on typical thermal smart materials such as nanoparticle suspensions, phase change materials, polymers, layered materials tuned by electrochemistry and other materials tuned by a specific external field. After surveying the fundamental mechanisms, we present applications of thermal smart components and devices in temperature control, thermal circuits, phonon computers, thermal metamaterials, and so on. Finally, we discuss the limitations and challenges of thermal smart materials, as well as our predictions for future development.

**thermal smart material, thermal conductivity, smart tuning, thermal control system**

**PACS number(s):** 44.10.+i, 44.90.+c, 65.20.+w

**Citation:** Z. T. Zhang, and B. Y. Cao, Thermal smart materials with tunable thermal conductivity: Mechanisms, materials, and applications, *Sci. China-Phys. Mech. Astron.* **65**, 117003 (2022), <https://doi.org/10.1007/s11433-022-1925-2>

## 1 Introduction

The demand for active and effective management of heat transfer is increasing in various up-to-date application scenarios [1-3]. The operating environment and requirements for heat transfer in modern devices are increasingly diversified and complicated, as shown in Figure 1, which has become a bottleneck for technological breakthroughs. The size of controlled objects ranges from macro- to micro/nanoscale, with heat flux changing substantially. For example, microelectronic devices (e.g., IC chips) with nanometer-scale dimensions have a high magnitude of power dissipa-

tion, with a maximum limit of more than  $400 \text{ W cm}^{-2}$ . It has been the key factor limiting the advances in this field since the junction temperature of chips must be kept within a particular range [4,5]. Meanwhile, rigorous thermal insulation is required in long-distance and large-scale pipeline fluid transport to minimize energy dissipation at the interface between the pipeline and containing liquid [6]. Rather than single requirements for heat dissipation or insulation, drastic heat flux fluctuations and ambient temperature variations, including extremely high/low temperatures in outer space, impose a critical request on the thermal management system of spacecraft. Variable orbital types and temperature-sensitive loading equipment require spacecraft to maintain a constant temperature despite differences in space heat flux

\*Corresponding author (email: [caoby@tsinghua.edu.cn](mailto:caoby@tsinghua.edu.cn))

[7]. Batteries, vehicles, and building envelopes all have similar requirements [8,9]. In summary, when the heat source power or ambient temperature varies over time, the temperature of devices will fluctuate sharply if the thermal management system cannot react in a timely manner. Traditional passive thermal control technology manipulates heat transfer between the operating system and the environment by optimizing the structure and layout of devices using thermal coatings and other functional materials. However, it is open-loop, which implies that the thermal management system cannot obtain the temperature feedback of devices and respond to the fluctuation of environmental temperature in real time. The active thermal control technology now available (e.g., electric heaters) has problems such as high energy consumption and limited life [2,10,11]. Compared with passive and active thermal control technologies, advanced and smart thermal control technologies are a potential solution for improved heat flux management. Thermal switches, thermal regulators, and thermal transistors [3,5,12,13] are examples of smart devices that people have invented with dynamic and controllable characteristics of thermal transport. Among the design principles of these advanced components, smart and reversible tuning of the thermal conductivities of materials lies at the core, requiring switching between the on (high) and off (low) states or a continuous variation of the conductivity values, as shown in Figure 2.

There is some experimental research on thermal smart materials for improving thermal management systems. Several mechanisms and experimental realizations have been reported regarding the reversible manipulation of thermal conductivities. Many methods and experimental realizations have been documented. Thermal smart materials require an external trigger, which could induce a drastic change in their thermal conductivities dramatically. The most critical performance parameter of thermal smart materials is the thermal switching ratio  $r$ , which is defined as the ratio of two thermal conductivities with or without stimuli:

$$r = \frac{k_{\text{on}}}{k_{\text{off}}}, \quad (1)$$

where  $k_{\text{on}}$  and  $k_{\text{off}}$  are the maximum and minimum thermal conductivities of thermal smart materials, respectively. In addition to  $r$ , response time,  $\tau$ , namely the transition process time between the on and off states, is also an important performance parameter.

In this paper, we briefly review the research advancement of thermal smart materials in recent years. Sect. 2 surveys several typical types of thermal smart materials in terms of their fundamental physical mechanisms, thermal switching ratio, and application value. After discussing the fundamental mechanisms, we present applications of thermal smart devices based on thermal smart materials in sect. 3,

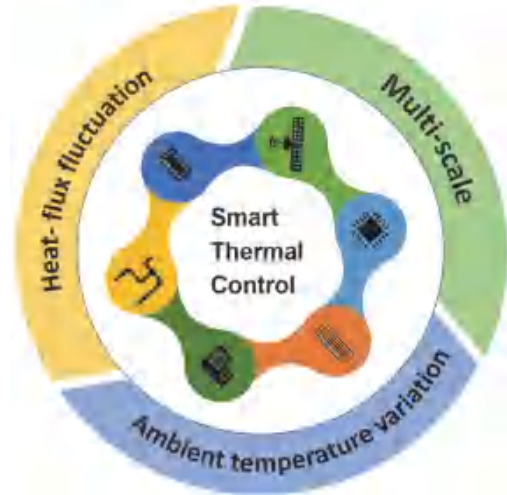


**Figure 1** (Color online) Challenge in thermal management systems. In different fields, multiscale systems under the situation of variable heat flux and extreme temperatures require active and smart thermal control technologies.

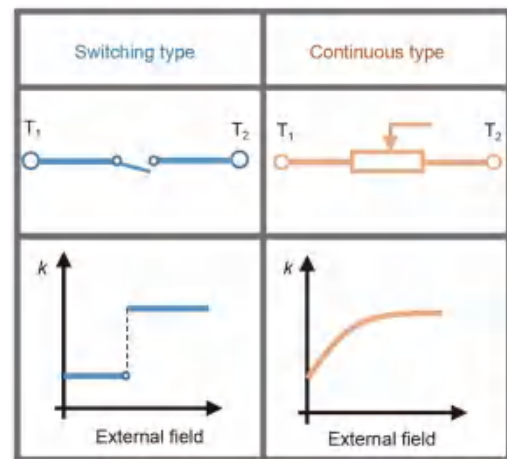


**Figure 2** (Color online) Schematic of switching and continuous thermal smart materials.

such as temperature control devices, typical thermal circuits (e.g., solid-state refrigeration), thermal metamaterials, and even phonon computing. Finally, we discuss the difficulties and challenges of thermal smart materials in sect. 4 and provide a forecast for future development.

## 2 Mechanisms of thermal smart materials

### 2.1 Nanoparticle suspensions

Low-dimensional materials, such as graphene flakes and carbon nanotubes, have excellent thermal properties [14,15]. These anisotropic nanoparticles have high thermal conductivities in a specific direction. For example, the axial thermal conductivity of carbon nanotubes could be larger than  $1000 \text{ W m}^{-1} \text{ K}^{-1}$ . Accordingly, suspensions composed

of nanoparticles with high thermal conductivity nanoparticles and fluids are expected to improve the thermal conductivity of the base fluid. However, previous experimental results suggested that the enhancement of thermal conductivity by incorporating nanoparticles into fluids is limited [16,17]. The anisotropy of low-dimensional nanoparticles leads to their high thermal conductivity only when they are oriented in a certain direction. These particles are distributed randomly in terms of both spatial positions and orientations in liquid solutions without external fields. In addition, interfacial thermal resistance between nanoparticles and the surrounding fluid also limits the improvement of the thermal conductivity of suspensions [9,18]. It is notable that these anisotropic particles prefer to align along the field direction and form chain-like structures under external fields such as electric fields [19], magnetic fields [20], or shear flow [21], leading to anisotropic electric conductivity or shear thinning behavior [22]. These findings show that the thermal conductivity of the suspension should also be tunable by manipulating nanoparticles with these external fields [23,24]. The dynamics of these particles are governed by translational and rotational Brownian diffusion at equilibrium [25], while the application of some external field will restrict the random motion and orient the particles in a specific direction [26,27]. Using an electric field as an example, the particles are polarized to form dipoles, which can be further coupled with the field to generate torque to orient the particles along the electric direction, making them migrate to the electrodes due to dielectrophoresis and form end-to-end contacts due to Coulomb forces [27,28]. As shown in Figure 3(a), these chain structures could form effective thermal conductive pathways, and heat can be largely transferred through the network, leading to the anisotropy of thermal conductivity. The thermal conductivity in the direction of the electric field is higher than that in other directions. If the suspended particles create a conductive network, theoretical models for nanoparticle suspensions also anticipate an increase in thermal conductivity [29,30].

On this basis, Zhang et al. [31] fabricated graphene na-

nosheets/Mg-Al layered double hydroxides (GNS/LDH) suspended in silicone oil. When a DC electric field is applied, the particles gradually pack into small ordered chains along the electric field direction and eventually form long chains, as shown in Figure 3(b). The largest switching ratio of thermal conductivity is approximately  $r = 1.35$ , with a particle volume fraction of 15% when the electrical field strength is  $E = 700$  V/mm. The switching ratio slightly decreases to  $r = 1.28$  after a few cycles and then becomes unchanged, as shown in Figure 3(c). The thermal conductivity of the nanoparticle suspension is also tuned using a magnetic field. Raj's group [32-34] performed systematic experimental studies with  $\text{Fe}_3\text{O}_4$  ferromagnetic nanoparticles suspended in an organic solution controlled by a magnetic field. Similar to the above discussion, the ferromagnetic particles formed chains and aligned in the direction of the magnetic field as the magnetic field increased, leading to an improvement in the thermal conductivity of the suspensions. The obtained switching ratio is as large as  $r = 2.5$  when the magnetic field strength is  $B = 82$  G. Altan et al. [35] have proved that enhancement of the thermal conductivity of a  $\text{Fe}_3\text{O}_4$  suspension results in a switching ratio of  $r = 1.07$ . To get a greater switching ratio, some researchers have used carbon nanoparticles (e.g., graphene nanosheets) with higher thermal conductivity and a larger aspect ratio to substitute ferromagnetic particles. Ding's group [36] used graphite nanoflakes suspended in a Poly-Alpha-Olefin solution as a research system, achieving  $r = 3.25$  with 0.8% (w/w) magnetic graphene at  $B = 425$  G. After several cycles, the switching ratio might still approach  $r = 3.0$ . Table 1 summarizes the major features of the reviewed nanoparticle suspensions. Due to the excellent properties of nanoparticles, suspensions as thermal smart materials have a short response time, low energy consumption, excellent reversibility, and can continuously adjust the thermal conductivity.

## 2.2 Layered materials using intercalation

The microstructure of certain layered materials can be altered

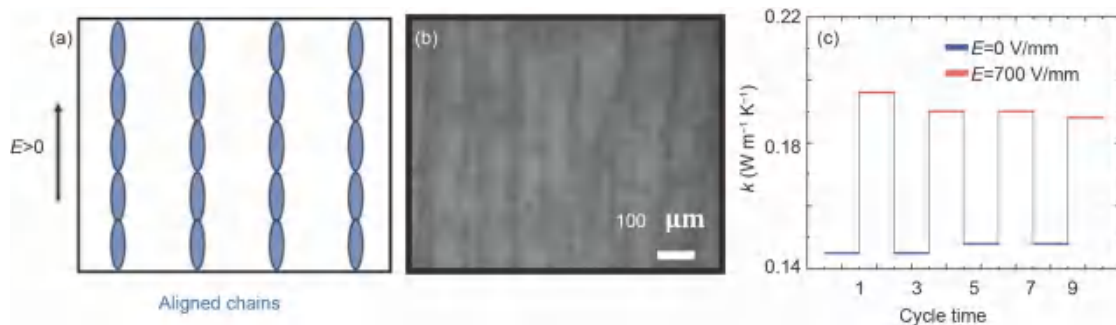


**Figure 3** (Color online) Schematic, microstructure, and reversibility tests of the GNS/LDH suspension under a DC electrical field. (a) Chain structures align along the direction of the electrical field, forming effective thermal conductive paths. (b) Microstructure of the GNS/LDH suspension under a DC electrical field.  $E = 300$  V/mm. (c) Reversibility testing of the thermal conductivity of the GNS-LDH suspension under the on/off cycles of a DC electric field [31].

**Table 1** Overview of nanoparticle suspensions

| Nanoparticle                       | Fluid             | External field   | Thermal conductivity without external field $k_0$ ( $\text{W m}^{-1} \text{K}^{-1}$ ) | Thermal switching ratio $r$ | Type       | Ref. |
|------------------------------------|-------------------|------------------|---|-----------------------------|------------|------|
| Graphene/layered double hydroxides | silicon oil       | electrical field | 0.15  | 1.4                         | continuous | [31] |
| $\text{Fe}_3\text{O}_4$ (6.7 nm)   | kerosene          | magnetic field   | 0.14  | 2.5                         | continuous | [32] |
| $\text{Fe}_3\text{O}_4$ (6.7 nm)   | hexadecane        | magnetic field   | 0.17  | 2.2                         | continuous | [33] |
| $\text{Fe}_3\text{O}_4$ (10 nm)    | kerosene          | magnetic field   | 0.15  | 1.5                         | continuous | [34] |
| Graphene                           | Poly-Alpha-Olefin | magnetic field   | 0.17  | 3.3                         | continuous | [36] |

by intercalating additional atoms into the atomic planes of the materials. Generally, intercalating atoms into the lattices of layered materials induces lattice defects that enhance the phonon scattering effects, reducing the thermal conductivity of layered materials [37]. Some experimental studies [38,39] have indicated that permanent intercalation could affect the thermal conductivity of layered materials. For example, the thermal conductivity of molybdenum disulfide [38] can be modified by electrochemical intercalation. With increasing lithium-ion concentration, the thermal conductivity of  $\text{MoS}_2$  decreased by four-fifths due to compositional and structural changes caused by lithiation, as shown in Figure 4(a). In addition to lattice defects, intercalation can change the lattice type of certain layered materials, leading to a variation in thermal conductivity [40]. Recently, the static and permanent insertion has gone even further to dynamic and reversible processes by electrochemical techniques, implying that the thermal conductivity of layered materials could be tunable by manipulating intercalated atoms.

$\text{LiCoO}_2$  was considered first because of its reversible lithiation characteristics. Cho et al. [41] suggested a reversible thermal conductivity  $\text{LiCoO}_2$  electrode for an electrochemical cell, achieving a thermal switching ratio of  $r = 1.5$ . During the charge-discharge cycling, the  $\text{LiCoO}_2$  electrode delithiated from  $\text{Li}_{1.0}\text{CoO}_2$  to  $\text{Li}_{0.6}\text{CoO}_2$  within approximately 6 h at a working voltage of  $U = 4.2$  V. These two distinct phase states (lithiated states and partial lithiated states) have different thermal conductivities [42]. Furthermore, phonon scattering is also enhanced with increasing Li vacancies, contributing equally to the decrease in thermal conductivity. Similarly, the thermal conductivity affected by  $\text{Li}^+$  concentration in the charge-discharge process was observed for the two-dimensional van der Waals material black phosphorus [43] presented in Figure 4(b), which also has a high capacity for lithium-ion intercalation [44]. Lithium ions could reversibly intercalate into black phosphorus during the charge-discharge process. With increasing  $\text{Li}^+$  concentration, the in-plane and out-plane thermal conductivity both decreased because the inserted Li atoms worked as scattering sources for phonons in black phosphorus. The maximum thermal switching ratio was as large as  $r = 1.6$ , with a response time of over tens of hours. Goodson's group [45]

demonstrated reversible thermal conductivity modulation of nanoscale  $\text{MoS}_2$  films actuated by reversible electrochemical intercalation of lithium ions. When Li atoms intercalate into the  $\text{MoS}_2$  layers, the inserted atoms increase phonon scattering, decrease phonon lifetime, and induce a  $c$ -axis tensile strain [46]. The additional strain reduces the group velocity of the phonons. Furthermore, the system partially transforms from the 2H phase (pristine  $\text{MoS}_2$ ) into the 1T phase (Li-intercalated  $\text{MoS}_2$ ) during the charging process, creating 2H-1T phase boundaries along the  $c$ -axis [38], and leading to additional phonon scattering. As a result, the thermal switching ratio is close to  $r = 10.0$ . Yildiz's group [47] stepped forward to bi-directionally control thermal conductivity based on the tri-state phase transition of  $\text{SrCoO}_x$  (SCO), as shown in Figure 4(c). The brownmillerite  $\text{SrCoO}_{2.5}$  (BM-SCO) was oxygenated to perovskite  $\text{SrCoO}_{3-\delta}$  (P-SCO) via applying an anodic bias, increasing the thermal conductivity with  $r = 2.5$ , and was hydrogenated to H- $\text{SrCoO}_{2.5}$  (H-SCO) with a cathode bias, effectively reducing the thermal conductivity with  $r = 4.0$ . When comparing BM-SCO with P-SCO, the latter has higher lattice symmetry, fewer oxygen vacancies, and a lower lattice constant [48,49]. This contributes to a decrease in phonon scattering and an increase in thermal conductivity. The H-SCO retained the original brownmillerite lattice structure but introduced hydrogen atoms as lattice defects [40], resulting in the lowest thermal conductivity of the three. The thermal switching ratio is  $r = 10$ , and the response time is approximately 40 min. Table 2 summarizes the key characteristics of the reviewed layered materials. The primary problem with tuning layered materials by using electrochemical methods is their long response time. Due to the slow process of ions in and out of lattices, the tuning process may be as long as tens of minutes or even hours. Future research should focus on developing materials that have faster response times to adapt to the rapid-changing heat flux in microelectronic devices.

### 2.3 Phase change materials

When the ambient temperature reaches a critical threshold and a phase transition occurs, the microstructure of the phase change material (PCM) changes, resulting in a sudden shift

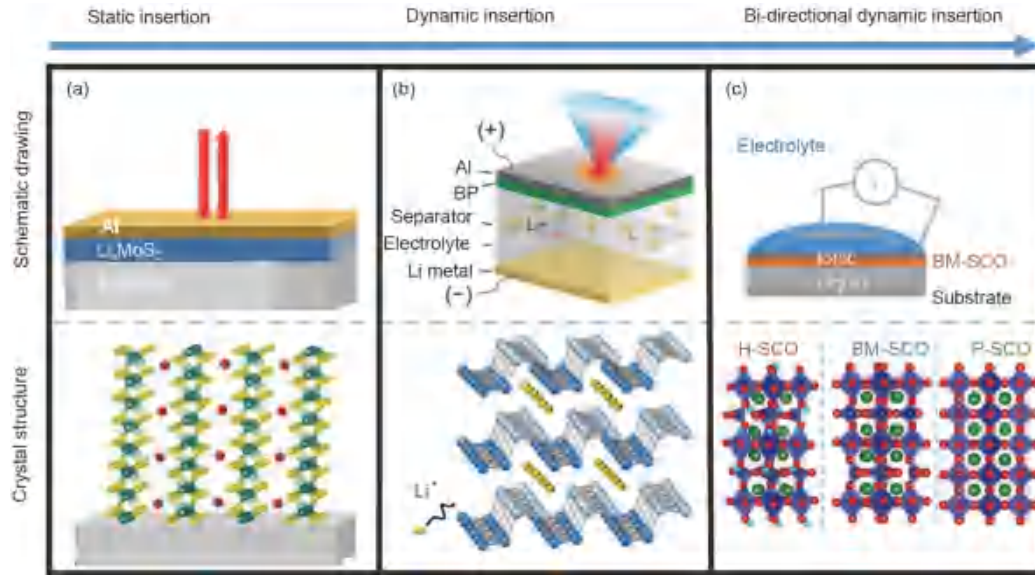


**Figure 4** (Color online) Schematic (upper) and crystal structure (lower) of typical layered materials with electrochemical control. (a) MoS<sub>2</sub> [38]; (b) black phosphorus [43]; (c) SCO [47].

**Table 2** Overview of layered materials

| Material           | Responding time $\tau$ (h) | Thermal conductivity without charging $k_0$ ( $\text{W m}^{-1} \text{K}^{-1}$ ) | Thermal switching ratio $r$ | Type       | Ref. |
|--------------------|----------------------------|---|-----------------------------|------------|------|
| LiCoO <sub>2</sub> | 3.0                        | 5.4   | 1.5                         | continuous | [41] |
| Black phosphorus   | 36.0                       | 4.0   | 1.6                         | continuous | [43] |
| MoS <sub>2</sub>   | 0.25                       | 16.0  | 10.0                        | continuous | [45] |
| SCO                | 0.67                       | 1.7   | 10.0                        | continuous | [47] |

in the thermal conductivity [50]. The PCM will return to its original state again if the ambient temperature rises or drops to the original level, making it a good candidate for thermal smart materials. According to the phase transition types, PCMs can be divided into four categories: solid-liquid, solid-solid, solid-gas, and liquid-gas PCMs [51]. Solid-solid and solid-liquid PCMs have received increased attention as a result of the huge volume shift in the solid-gas and liquid-gas phase transition processes. Solid-solid PCMs, including metal-insulator transition materials, magnetostructural transition materials, and phase-change memory materials, have stable physical states and properties, enabling them to be used in a broad range of applications. Solid-liquid materials are mainly composite materials composed of organic fluids and solid particles that have high thermal conductivity. Different types of nanoparticles might be added to the base fluid to provide different phase transition points and thermal switching ratios.

### 2.3.1 Metal-insulator transitions

The metal-insulator transition (MIT) can tune the electrical conductivity of certain materials drastically. VO<sub>2</sub> is a well-known MIT material [52] whose electrical conductivity  $\sigma$

may change by five orders of magnitude at the phase transition temperature  $T = 340$  K. Considering the Wiedemann-Franz (WF) law, which illustrates that electrons and phonons make the same magnitude of contributions to the thermal conductivity in the metallic state and only phonon conduction dominates in the insulating state, the thermal conductivity of VO<sub>2</sub> in the MIT process is expected to change dramatically. However, the thermal conductivity of VO<sub>2</sub> bulk materials remains almost unchanged around the phase transition point [53,54]. Xie et al. [55] developed a single-crystal VO<sub>2</sub> nanobeam structure but only achieved a thermal switching ratio of  $r = 1.1$  at  $T = 340$  K within several seconds, despite the fact that it possessed high electrical conductivity in the metallic state. Dahal et al. [56] proposed a V-VO<sub>2</sub> core-shell structure with a thermal switching ratio of  $r = 1.2$  at  $T = 340$  K. Electrons transferred from the metallic V to the surrounded metallic VO<sub>2</sub>, leading to a higher electron thermal conductivity  $k_{el}$ . Kizuka et al. [57,58] indicated that the thermal switching ratio of polycrystalline VO<sub>2</sub> films at  $T = 340$  K might reach as large as  $r = 1.6$  in the cross-plane direction. These results are not as high as expected; the possible explanations may be that the phonon thermal conductivity  $k_{ph}$  decreases in the transition to the metallic state,

although the electron thermal conductivity  $k_{el}$  increases as the WF law predicts, or that the WF law is not valid in the metallic state [53,54]. Lee et al. [59] discovered that phonon thermal conductivity,  $k_{ph}$ , remains almost unchanged throughout the MIT process and that electrons in the metallic state contribute substantially less than the WF law anticipated by the first-principles method. Furthermore, the phase transition temperature of VO<sub>2</sub> decreased to  $T = 310$  K, and a thermal switching ratio of  $r = 1.5$  was achieved if the VO<sub>2</sub> nanobeam was doped with a few percent W [59], as shown in Figure 5(a). The authors indicated that the VO<sub>2</sub> in the metallic state tends to behave as WF laws predict, with increasing W concentration.

### 2.3.2 Magnetostructural transitions

Heusler alloys are magnetic intermetallics with face-centered cubic crystal structures that exhibit unique properties such as magnetoresistance, ferrimagnetism, and semimetallicity [60,61]. At the phase transition temperature, a structural transformation of Heusler alloys from paramagnetic austenite to ferromagnetic martensite occurs, which may be recognized as a magnetostructural first-order phase transition. The behavior of  $k_{el}$  throughout the transition process correlates with the behavior of  $\sigma$ : it increases sharply when the temperature rises above the critical point. This phase transition might potentially result in the formation of twin boundaries, which would increase phonon scattering while decreasing thermal conductivity. Batdalov et al. [62] proposed a Ni<sub>45.37</sub>Mn<sub>40.91</sub>In<sub>13.72</sub> alloy with a thermal switching ratio of  $r = 1.6$  at  $T = 325$  K. Zheng et al. [63] discovered that Mn<sub>x</sub>MGe (M = Co, Ni) alloys transformed from the martensitic to austenitic phase, with the phase transition temperature varying between 300-600 K depending on the material composition. The maximum thermal switching ratio is  $r = 1.4$  for Mn<sub>1.014</sub>NiGe at  $T = 600$  K. A similar behavior was also observed in Mn<sub>1.007</sub>CoGe with  $r = 1.2$ . Zheng et al. [64] later presented a new type of Heusler alloy, the polycrystalline NiMnIn alloy shown in Figure 5(b), achieving  $r = 1.7$  at  $T = 320$  K.

### 2.3.3 Phase change memory

Chalcogenide phase-change memory materials, such as Ge<sub>2</sub>Sb<sub>2</sub>Te<sub>5</sub> (GST), GeTe<sub>4</sub>, and GeTe, may switch between crystalline and amorphous states at room temperature [65]. The phase change memory material is amorphous at low temperatures in which the coherences (coupling of vibrational modes) make the greatest contribution to heat conduction, resulting in poor thermal conductivity [66]. At the phase transition temperature, it turns into a hexagonal phase, in which electrons contribute more to heat conduction, increasing its thermal conductivity [67]. Fast cooling will cause phase change memory material to become amorphous at room temperatures, while fast heating causes phase change memory material to crystallize again above the transition temperature. The thermal conductivity of GST can change by a factor of 7.5 at room temperature [68]. Reifenberg et al. [69] reported an increase in  $k$  as large as  $r = 3.0$  for GST films at  $T = 298$  K. Ghosh et al. [70] demonstrated a GeTe film with  $r = 6.2$  at  $T = 453$  K, as shown in Figure 5(c).

### 2.3.4 Composite materials

Composite materials with liquid-solid phase transitions have switchable thermal conductivities. As shown in Figure 6, Zheng et al. [71] first began their investigation using a graphene/hexadecane hybrid. They observed that the graphene sheets contacted each other, formed agglomerates, and clustered the grain boundary across the phase transition of hexadecane, establishing a thermal conductive network. The thermal conductivity of the composite is increased by the effective thermal conductive network, resulting in a thermal switching ratio of  $r = 3.2$  at  $T = 291$  K. The switching ratio did not change significantly after several cycles. Many experimental measurements [72-77] for different liquids and containing particles were performed, also achieving  $r$  in the range of 1.5-3.5.

The key characteristics of the reviewed phase change materials are summarized in Table 3. Because the PCMs are activated by ambient temperature, they are excellent for adaptive adjustment. However, the phase transition tem-

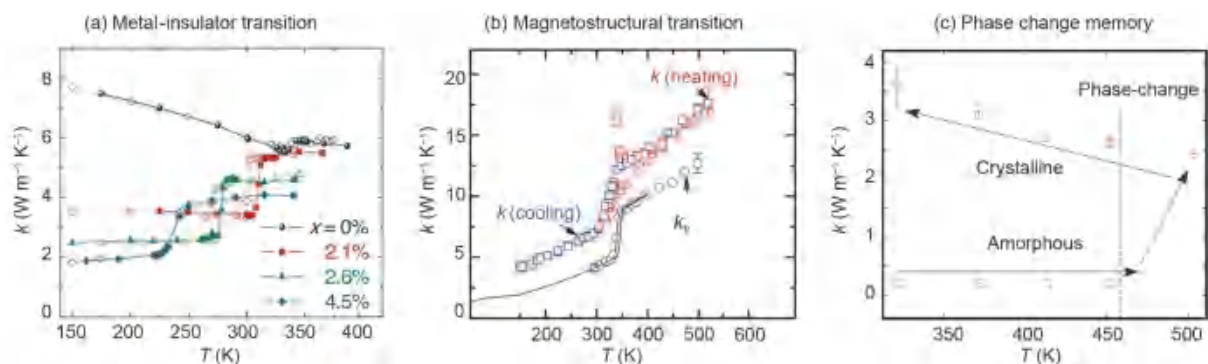


**Figure 5** (Color online) Thermal conductivity variation of solid-solid phase change materials as a function of temperature. A sharp change in thermal conductivity occurs at the phase transition point. (a) VO<sub>2</sub> doped with W, where  $x$  is the volume content of W [59]; (b) Ni-Mn-In alloy [64]; (c) GeTe [70].

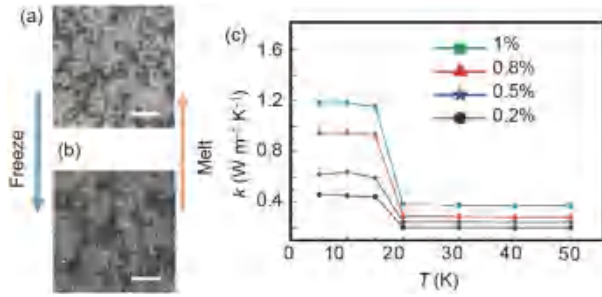


**Figure 6** (Color online) Liquid-solid phase change materials. (a) Optical images of melted graphite-hexadecane composite. (b) Optical images of the frozen graphene-hexadecane composite. The graphene contacted better and clustered along the grain boundary when frozen. The scale bar is 200  $\mu\text{m}$ . (c) Thermal conductivity variation of the composite as a function of temperature [71].

perature for a specific PCM is fixed and usually deviates from room temperature. Although changing the proportion of components may control the phase transition temperature of certain PCMs, it is still a significant problem to be resolved.

## 2.4 Polymers

The state of soft matter, especially polymers, lies between

solids and perfect fluids and includes various kinds of systems which can deform or change microstructure in response to the environmental stimuli of varying magnitudes of thermal fluctuations [78]. As shown in Figure 7, the polymers could respond sensitively to the stimuli with an energy scale comparable to room temperature thermal energy, implying that minor external effects, including light excitation, electrical and magnetic effects, pressure and temperature gradient, could cause a significant and reversible change in the structure and performance of them [79]. This characterization makes it an excellent and outstanding candidate for thermal smart materials.

Shin et al. [80] produced a light-responsive azobenzene polymer with a thermal conductivity that could switch between high and low thermal conductivity states under UV and green light illumination. As shown in Figure 7(a), when exposed to UV light, the azobenzene groups of the polymer transform from trans state to cis state, leading to changes in the  $\pi$ - $\pi$  stacking geometry and driving the crystal-to-liquid phase transition. When exposed to green light, the azobenzene groups return to the planar state again, resulting in a switching ratio of  $r = 3.5$ . Li et al. [81] proposed poly(N-isopropylacrylamide) (PNIPAM) as a thermoresponsive

**Table 3** Overview of phase change materials

| Material  | Mechanism                    | Phase transition temperature $T_c$ (K) | Thermal conductivity below $T_c$ , $k_0$ ( $\text{W m}^{-1} \text{K}^{-1}$ ) | Thermal switching ratio $r$ | Type      | Ref. |
|---|------------------------------|--|--|-----------------------------|-----------|------|
| $\text{VO}_2$ nanobeam                                | MIT                          | 340                                    | 13.0   | 1.1                         | switching | [55] |
| V- $\text{VO}_2$ core-shell structure                 | MIT                          | 340                                    | 8.1  | 1.2                         | switching | [56] |
| $\text{VO}_2$ polycrystalline film                    | MIT                          | 340                                    | 3.6  | 1.6                         | switching | [57] |
| $\text{VO}_2$ doped with W                            | MIT                          | 310                                    | 3.8  | 1.5                         | switching | [59] |
| $\text{Ni}_{45.37}\text{Mn}_{40.91}\text{In}_{13.72}$ | magnetostructural transition | 325                                    | 5.8  | 1.6                         | switching | [62] |
| $\text{Mn}_{1.014}\text{NiGe}$                        | magnetostructural transition | 600                                    | 11.0   | 1.4                         | switching | [63] |
| $\text{Mn}_{1.007}\text{CoGe}$                        | magnetostructural transition | 600                                    | 7.0  | 1.2                         | switching | [63] |
| $\text{Ni}_{51.7}\text{Mn}_{34.3}\text{In}_{13.9}$    | magnetostructural transition | 320                                    | 7.5  | 1.7                         | switching | [64] |
| $\text{Ge}_2\text{Sb}_2\text{Te}_5$                   | phase change memory          | 300                                    | 0.2  | 7.5                         | switching | [68] |
| GeTe  | phase change memory          | 453                                    | 0.4  | 6.2                         | switching | [70] |
| Graphene/hexadecane                                   | solid-liquid transition      | 291                                    | 1.2  | 3.2                         | switching | [71] |
| Inverse micelle/hexadecane                            | solid-liquid transition      | 291                                    | 0.2  | 1.6                         | switching | [72] |
| Copper nanowire/hexadecane                            | solid-liquid transition      | 291                                    | 0.2  | 2.3                         | switching | [73] |
| Carbon nanotube/sodium deoxycholate                   | solid-liquid transition      | 300                                    | 0.2  | 2.9                         | switching | [74] |
| Carbon nanotube/hexadecane                            | solid-liquid transition      | 291                                    | 0.2  | 3.0                         | switching | [75] |
| Graphite nanofiber/paraffin                           | solid-liquid transition      | 329                                    | 0.4  | 1.8                         | switching | [76] |
| Carbon black/octadecane                               | solid-liquid transition      | 303                                    | 0.2  | 3.3                         | switching | [77] |

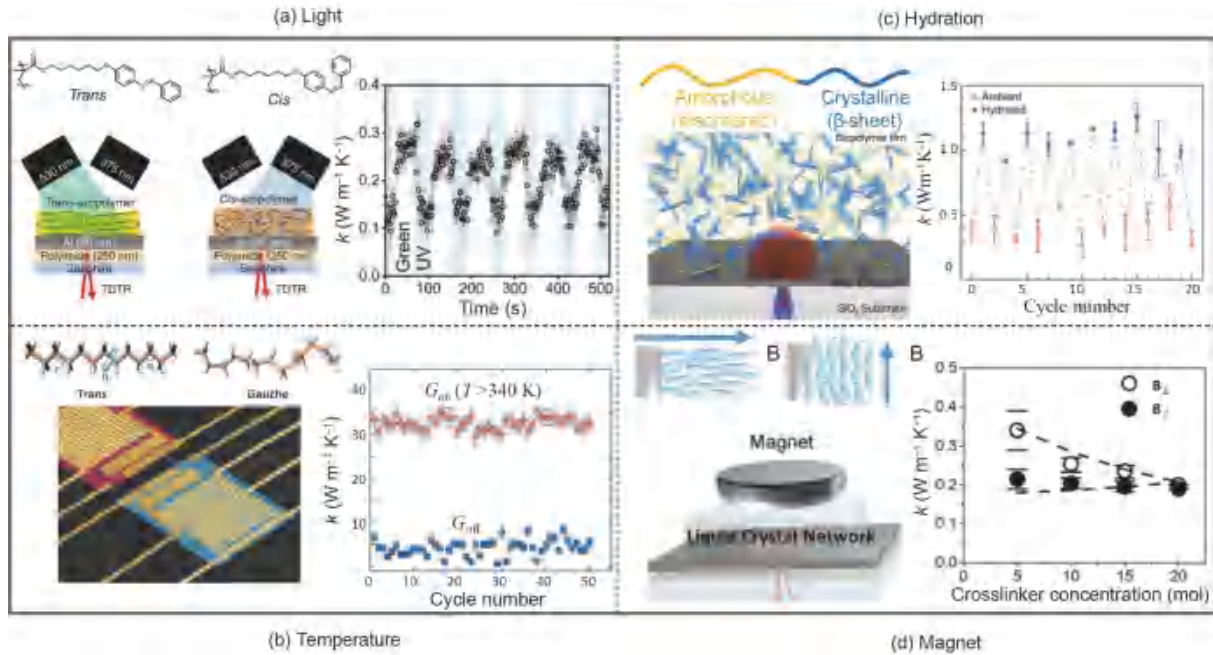


**Figure 7** (Color online) Diagram of polymers with different external excitations. (a) Azobenzene polymers [80]; (b) polyethylene nanofiber [82]; (c) tandem-repeat protein [84]; (d) liquid crystal [85].

polymer aqueous solution with a dramatic change in thermal conductivity at the phase transition temperature, achieving a thermal switching ratio up to  $r = 1.15$  at  $T = 304$  K. The possible explanation for the observed change might be the breaking of the hydrogen bonds between PNIPAM and water. When these bonds are broken, the intramolecular interactions of PNIPAM dominate above the phase transition temperature. After the transitions, PNIPAM shrinks and expels water, increasing the interfacial thermal resistance and yielding a reduction of thermal conductivity. Shrestha et al. [82] also reported a crystalline polyethylene nanofiber as a PCM with tunable thermal conductivity, as shown in Figure 7(b). The structural transition occurring at the phase transition temperature causes a drastic change in the polymer from a trans state to a combined trans-gauche state, impacting the phonon transport in the polymer. A thermal switching ratio of  $r = 8.0$  at  $T = 430$  K was achieved across the structural phase transition. Zhang et al. [83] revealed that, at the phase transition, the segmented rotation of polyethylene polymer chains causes the chain structure to become disordered, affecting the phonon transfer along the chains and reducing the thermal conductivity via a simulation method. Tomko et al. [84] hypothesized a class of tandem repetition (TR) proteins that have variable thermal conductivities triggered by hydration. The TR proteins are composed of repeat units, including both crystalline and amorphous strands, as shown in Figure 7(c). In the ambient state, the heat transmission in the protein is restricted by the amorphous domains. Even though the crystalline domains have high thermal conductivity, phonon scattering in the amorphous domains will reduce the

thermal conductivity of whole proteins. When the TR proteins are hydrated, their thermal conductivity increases, achieving  $r = 4.0$ . The possible mechanisms are that the amorphous domains and the morphology of whole proteins are affected by hydration and TR and influence the heat transfer in whole chains. Shin et al. [85] prepared liquid crystal polymers by photopolymerizing the nematic monomers, as shown in Figure 7(d). When applying a magnetic field, the liquid crystal polymers align along the direction of the applied field, reaching a thermal switching ratio of  $r = 1.4$ . Table 4 summarizes the essential characteristics of the reviewed polymers. Polymers react well to a wide range of external stimuli, and their electrical, optical, and mechanical properties are tunable and useful in various applications. However, in the absence of an external field, their thermal conductivities are often relatively low.

## 2.5 Materials responding to a specific field

### 2.5.1 Electrical field

Although heat transfer in most materials is independent of electrical fields, certain ferroelectric materials that polarize spontaneously in the presence of an electrical field can be suitable candidates for thermal smart materials [86]. The ferroelectric materials are made up of numerous domains which have different polarization orientation directions. As shown in Figure 8(a), when an electrical field is applied, these domains will polarize and align along the direction of the electrical field. When the polarization reaches a maximum, almost all these domains align in the direction of the

**Table 4** Overview of polymers

| Material               | External field | Thermal conductivity without external field $k_0$ ( $\text{W m}^{-1} \text{K}^{-1}$ ) | Thermal switching ratio $r$ | Type       | Ref. |
|------------------------|----------------|---|-----------------------------|------------|------|
| Azobenzene polymer     | light          | 0.10  | 3.5                         | switching  | [80] |
| PNIPAM                 | temperature    | 0.61  | 1.2                         | switching  | [81] |
| Polyethylene nanofiber | temperature    | 5.14  | 8.0                         | switching  | [83] |
| TR protein             | hydration      | 0.25  | 4.0                         | switching  | [84] |
| Liquid crystal network | magnetic field | 0.20  | 1.4                         | continuous | [85] |

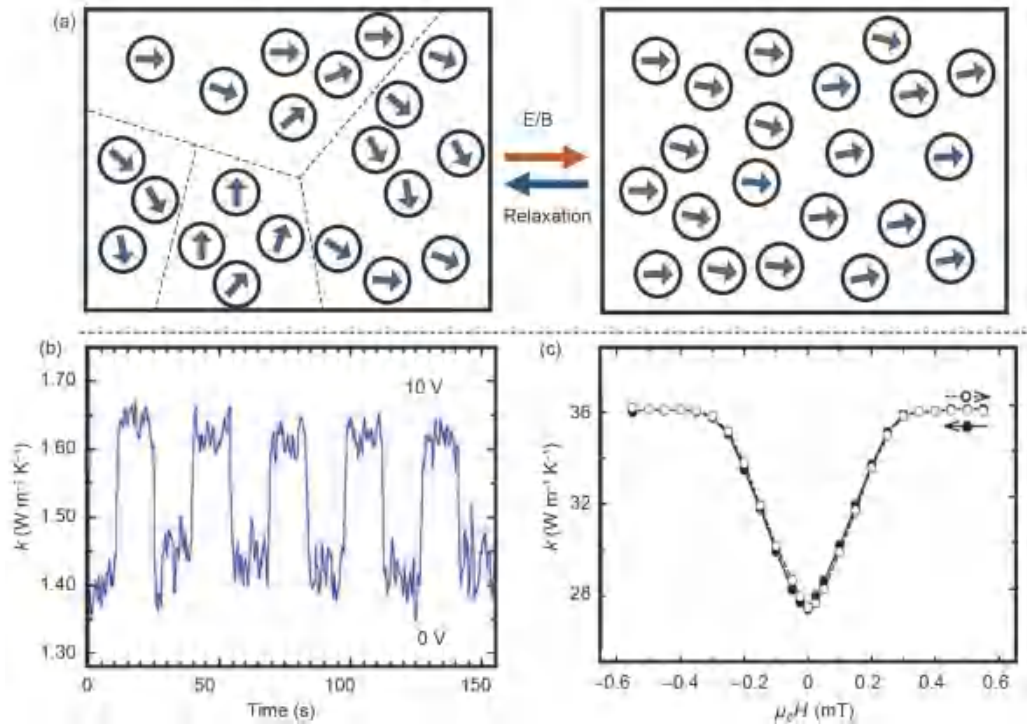


**Figure 8** (Color online) Typical materials tuned by an electrical/magnetic field. (a) Change in domains with an external field in ferroelectric/ferromagnetic materials. These materials consist of many domains with randomly spontaneous polarization directions. When applying an external field, these domains polarize and align in a similar direction along the external field, and the domain wall density decreases. Removing the external field, these domains orient themselves randomly again. (b) Thermal conductivity variation of PZT film as a function of time with electrical field switching [88]. (c) Thermal conductivity variation of the Co/Cu multilayer film as a function of magnetic field [94].

electrical field, and the domain wall density decreases. Because domain walls scatter phonons in the same way as grain boundaries, the decrease in their density could improve heat transmission in ferroelectric materials and increase their thermal conductivity [87,88]. Based on that, Ihlefeld et al. [89] achieved active and reversible tuning of thermal conductivity by manipulating the nanoscale ferroelastic domain structure of a  $\text{Pb}(\text{Zr}_{0.3}\text{Ti}_{0.7})\text{O}_3$  bilayer film. An improvement in thermal conductivity as large as  $r = 1.08$  was observed when  $E = 475$  kV/cm. Foley et al. [88] also observed a similar phenomenon for a PZT film with  $r = 1.13$  when  $E = 100$  kV/cm, as shown in Figure 8(b). Yiğen and Champagne [90] demonstrated thermal modulation of graphene suspended on a Si/SiO<sub>2</sub> substrate. A thermal switching ratio of  $r = 2.0$  was observed when the voltage  $U = 5$  V. The possible mechanism is that electrons moved as heat carriers in the

graphene and substrate, and their numbers increased when the bias was applied, causing  $k_{\text{el}}$  to improve. Some ferroelectric materials' thermal conductivity changes as a result of ferroelectric phase transitions caused by an electrical field. Kalaidjiev et al. [91] changed the thermal conductivity of triglycine sulfate to  $r = 1.2$  with  $E = 4.2$  kV/cm by applying an electrical field, which caused a second-order ferroelectric phase transition change, leading to the change in the thermal conductivity. The electrical field probably causes a leveling of curve slopes at energies of acoustic and long-wavelength transverse optical vibrations. Deng et al. [92] used an electrical field to manipulate the atomic structure of the organic ferroelectric material polyvinylidene fluoride (PVDF) to change its thermal conductivity. The PVDF is polarized with the help of an electric field. When an electric field is applied, the inter-chain structure becomes highly ordered, which re-

duces phonon scattering and improves thermal conductivity. The thermal conductivity could be tuned to a value as large as  $r = 1.5$ . The authors [93] also found that the thermal conductivity of organic nylon could be tuned by regulating its hydrogen bond with an electrical field, and the thermal switching ratio could reach  $r = 1.5$ .

### 2.5.2 Magnetic field

Due to WF principles, the classical magnetoresistance (MR) model [94] predicts that the magnetic field reduces the electrical conductivity of metals or semiconductors and hence reduces the thermal conductivity. However, this effect can be ignored for most metals at room temperature [95]. MR effects are more visible in semiconductors. The thermal conductivity of bismuth-antimonide alloy, for example, has a thermal switching ratio of  $r = 1.2$  with  $B = 0.75$  T [96]. In addition to the standard MR effect, the giant magnetoresistance effect [97] drew a lot of interest. The effect occurs in materials that are composed of ferromagnetic domains separated by nonmagnetic layers. Because the ferromagnetic domains orient randomly in the absence of a magnetic field, the material's electrical conductivity is relatively low. When applying a magnetic field, the domains tend to align with the magnetic field direction, increasing electrical and thermal conductivity. Kimling et al. [98] found that the thermal conductivity of Co/Cu multilayer films could be as large as  $r = 1.4$  with  $B = 0.6$  T, and its response time is on the order of microseconds. Magnons, like electrons and phonons, are heat carriers in some ferromagnetic materials. Magnons are quasiparticles that collectively excite the spin structures of electrons in crystal lattices [99]. Magnons can carry both energy and lattice momentum. The properties of magnons can be tuned by applying a magnetic field. When applying a magnetic field over a critical value, magnons will be restricted from contributing to thermal transport, reducing the thermal conductivity of ferromagnetic materials. Dhara et al. [100] reported a thermal conductivity adjustable InAs nanowire, whose thermal switching ratio can be as large as  $r = 2.3$  with  $B = 6$  T. Similarly, Huang et al. [101] investigated a ferromagnetic Ni nanowire with  $r = 2.7$  when  $B = 0.2$  T. Some antiferromagnetic materials also exhibit thermal switching behaviors at extremely low temperatures. Zhao et al. [102] proposed an antiferromagnetic  $\text{Co}_3\text{V}_2\text{O}_8$  single-crystal that could operate at temperatures below 12 K. When a magnetic field is applied,  $\text{Co}_3\text{V}_2\text{O}_8$  transformed between paramagnetic and ferromagnetic states through a series of magnetic phase transitions. The phonon scattering is enhanced across the transition, and the thermal conductivity of  $\text{Co}_3\text{V}_2\text{O}_8$  is reduced, achieving a thermal switching ratio of approximately  $r = 100$ .

### 2.5.3 Strain

The external pressure may cause a configurational change in

certain materials, resulting in variations in their thermal properties. McGuire et al. [103] proposed a phase transition from fcc phase state to bcc state in a NaCl crystal induced by pressure, leading to  $r = 1.6$ . Talyzin et al. [104] reported phase transitions in  $\text{LiBH}_4$  structures, where the  $\alpha\text{-LiBH}_4$  transforms into  $\beta\text{-LiBH}_4$  when applying external pressure, as shown in Figure 9(a). When the pressure  $P = 0.7$  GPa, a switching ratio as large as  $r = 2.3$  was achieved. Some low-dimensional nanomaterials also show thermal switching behaviors with strain. Li et al. [105] used a molecular dynamics simulation method to investigate the effects of strain on the lattice thermal conductivity of low-dimensional silicon materials. The thermal conductivities of strained silicon nanowires and thin films were shown to decrease continuously when the strain changed from compressive to tensile because the mode-specific group velocities of the phonon-specific heat of each propagating phonon mode decreased continuously during the process, as shown in Figure 9(b). Yang et al. systematically studied the effects of strain on the thermal conductivity of one-dimensional nanomaterials, including molybdenum disulfide nanotubes [106], one-dimensional van der Waals heterostructures (carbon-boron nitride) [107], and epoxy resin [108,109]. The substantial change in thermal conductivity caused by axial strain is also on account of the decrease in phonon group velocity and phonon relaxation time, which is induced by increased phonon scattering. The strain effectively tunes the thermal conductivity of these one-dimensional materials, with a maximum switching ratio of  $r = 2.5$ . Zeng et al. [110] experimentally demonstrated this phenomenon with strained multilayer graphene, whose thermal conductivity decreased with  $r = 1.4$  when a tensile strain of 1% was applied. In addition, Du et al. [111] prepared a compressible graphene composite foam material. When compressing the composite to squeeze out the air in the pores (Figure 9(c)), the thermal conductive paths are formed, increasing the thermal conductivity of the composite. When the compression ratio is 80%, a switching ratio of  $r = 8.0$  can be achieved. The key aspects of the above materials that can be tuned by specific fields are summarized in Table 5.

## 3 Potential applications

Since we have fully discussed the mechanisms and performances of thermal smart materials, we now evaluate the potential applications of these materials in the industry. Thermal smart materials are the basis of thermal smart components and devices with dynamic and controllable heat transfer characteristics, including thermal switches, thermal resistors, and thermal regulators. A variable thermal resistor might adjust its thermal conductance continuously like a variable electrical resistor, thereby stabilizing the working

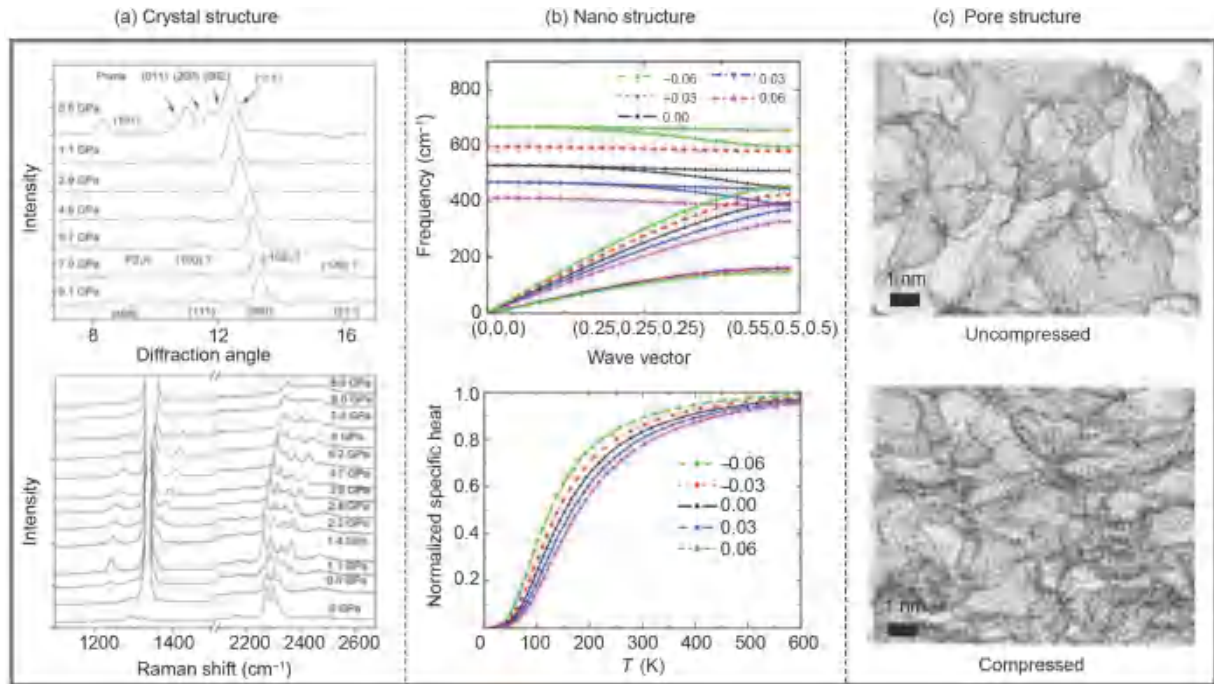


**Figure 9** (Color online) Structural change of typical materials under pressure. (a) LiBH<sub>4</sub>: XRD patterns and Raman spectra obtained during compression. These changes in peaks are interpreted in terms of a phase transition from ambient pressure  $\alpha$ -LiBH<sub>4</sub> to a high-pressure  $\beta$ -LiBH<sub>4</sub> phase [104]. (b) Silicon nanowires: phonon-dispersion curves and normalized specific heat of silicon nanowires under different strains, where negative value denotes compressive strain and positive value denotes tensile strain. Under tensile strain, both phonon group velocity and specific heat decrease [105]. (c) Graphene composite foam: the uncompressed and compressed states of composites [111].

**Table 5** Overview of materials tuned by specific fields

| Material   | External field   | Thermal conductivity without external field $k_0$ ( $\text{W m}^{-1} \text{K}^{-1}$ ) | Thermal switching ratio $r$ | Type       | Ref.  |
|--|------------------|---|-----------------------------|------------|-------|
| PZT film   | electrical field | 1.4   | 1.1                         | switching  | [88]  |
| Pb(Zr <sub>0.3</sub> Ti <sub>0.7</sub> )O <sub>3</sub> film  | electrical field | 1.2   | 1.1                         | switching  | [89]  |
| Si/SiO <sub>2</sub>  | electrical field | 2.0   | 2.0                         | continuous | [90]  |
| Triglycine sulfate   | electrical field | 4.1   | 1.2                         | switching  | [91]  |
| Polyvinylidene fluoride                                      | electrical field | 0.2   | 3.3                         | switching  | [92]  |
| Organic nylon  | electrical field | 0.3   | 1.5                         | switching  | [93]  |
| Bismuth-antimonide alloy                                     | magnetic field   | 3.2   | 1.2                         | continuous | [96]  |
| Co/Cu multilayer film  | magnetic field   | 18.0  | 2.0                         | continuous | [98]  |
| InAs nanowire  | magnetic field   | 0.2   | 2.5                         | continuous | [100] |
| Ni nanowire  | magnetic field   | 32.0  | 2.7                         | continuous | [101] |
| Co <sub>3</sub> V <sub>2</sub> O <sub>8</sub> single-crystal | magnetic field   | 1.0   | 100.0                       | continuous | [102] |
| NaCl crystal   | pressure         | 11.9  | 1.6                         | switching  | [103] |
| LiBH <sub>4</sub>  | pressure         | 1.5   | 2.3                         | switching  | [104] |
| Molybdenum disulfide nanotube                                | pressure         | 15.0  | 2.5                         | continuous | [106] |
| Carbon-boron nitride   | pressure         | 235.1   | 1.6                         | continuous | [107] |
| Epoxy resin  | pressure         | 0.1   | 2.2                         | continuous | [109] |
| Multilayer graphene  | pressure         | 551.0   | 1.4                         | continuous | [110] |
| Graphene composite foam                                      | pressure         | 50.0  | 8.0                         | continuous | [111] |
| Liquid metal foam  | pressure         | 5.1   | 3.5                         | continuous | [112] |

temperature of heat-generating devices or other equipment sensitive to temperature. The thermal conductivity of thermal switches might flip between the high (on) and low (off) states when activated by appropriate external fields. The thermal characteristics of the phase transition material-based thermal regulator might change with the ambient temperature. When a critical transition temperature is reached, the thermal conductance of the thermal regulator varies dramatically. Thermal switches and regulators are important components in certain thermal circuits that allow precise temporal and spatial heat flux control, thus conserving energy and improving energy efficiency. These thermal smart components are fundamental for designing thermal logic gates and thermal memory elements, providing the possibility for phononic computing. Furthermore, thermal smart materials may also be employed as thermal metamaterials, allowing them to perform additional functions.

### 3.1 Variable thermal resistor

Variable thermal resistors are the critical component of thermal control systems that demand continuous heat flux control to stabilize device operating temperature by tuning the thermal conductivities in real time. This thermal component has the potential to be used in batteries, spacecraft, vehicles, and thermal energy storage systems. Du et al. [111] demonstrated a variable thermal resistor using a compressible graphene foam composite that has open pores and an interconnected network. When compressing the composite and squeezing out the air in the pores, thermal conductive paths are generated, increasing the thermal conductivity of the composite. Partial compression makes any thermal conductance between the high and off state accessible. The setup of testing experiments is demonstrated in Figure 10(a). The environmental chamber results showed that the variable thermal resistor could keep the operating temperature consistent when the ambient temperature changed by 10 K or the heating power changed by 2.7 times. Similarly, Yu et al. [112] proposed a stretchable liquid metal foam elastomer composite with both tunable electrical and thermal conductivity under strain, as well as stretching-enhanced electromagnetic-interference shielding effectiveness. Due to conductive network elongation and reorientation, a thermal switching ratio of  $r = 16.0$  was achieved under a considerable strain of 400%. Stretchable electronics, such as wearable electronics, would benefit greatly from these properties of variable resistors [113]. Based on the phonon-folding scattering effect on large-area graphene [114,115], Song et al. [114] presented an instantaneously adjustable thermal resistor using foldable graphene. By folding and unfolding graphene through applied strain, a continuous change in thermal conductivity as large as  $r = 3.0$  can be achieved. Based on graphene/layered double hydroxides-silicon oil

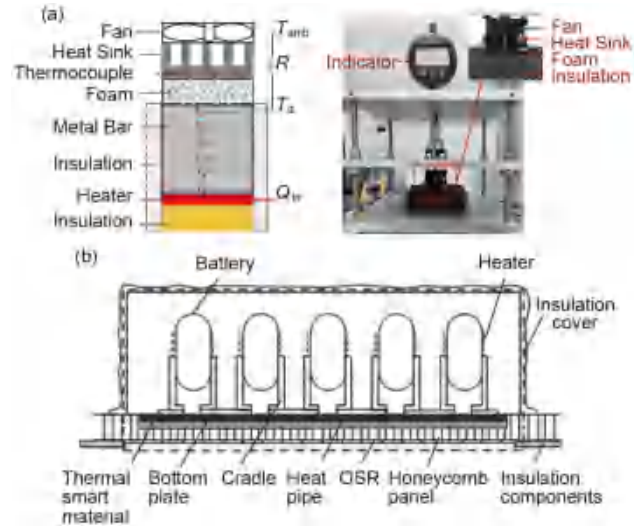


**Figure 10** (Color online) Variable thermal resistors. (a) Schematic of the testing experiments for the graphene composite resistor. The heater is installed on the insulating layers to prevent heat dissipation. The composite can be compressed to a different ratio by adjusting the middle plate [111]. (b) Schematic of the GNS/LDH resistor in the satellite battery installation structure. The thermal resistor is arranged between the bottom plate of lithium-ion batteries and the heat pipes [117].

nanoparticle suspensions, Cao et al. [31,116] designed a variable thermal resistor whose thermal conductivity can be tuned continuously by an electrical field. This thermal resistor was used in the lithium-ion battery module of a satellite thermal management system [117]. The diagram of the battery installation structure with a thermal resistor is shown in Figure 10(b). When the heat consumption of the battery changes, the strength of the electric field can be changed synchronously, which adjusts the thermal resistance of the resistor to maintain the operating temperature of the battery. The results of the on-orbit thermal analysis indicated that the temperature uniformity was improved by approximately 8%, while the heater power demand was reduced by more than 15% with the thermal resistor. In addition, the thermal resistor has no moving components, uses less energy, and has a quick response time.

### 3.2 Energy conservation

Air conditioning systems are widely used to keep indoor temperatures steady during the day and night for human activities; even the outdoor temperatures and conditions vary significantly. However, temperature control consumes a lot of energy—48% of total residential energy and 35% of total commercial energy [118]. Thermal smart devices, such as thermal switches, may be used to control the thermal conductance of building envelopes. Menyhart et al. [119] demonstrated the use of thermal smart materials in building envelopes via a simulation method. The authors assumed that materials with adjustable thermal conductivities could allow

building envelopes to be insulated during the day to prevent heat flow from the outside and conduct heat from the building at night. The performance of thermal smart materials varied drastically depending on the weather conditions, with the energy savings ranging from 7% to 42%. Koenders et al. [120] also presented how to use thermal switches as construction elements to reduce the energy consumption of building systems using a simulation method. The simulation results showed that it can achieve an  $r = 9.0$  compared with the insulating state. With thermal switches, over 70% fewer comfort exceedance hours were achieved, and the specific annual heating demand was reduced by about 20%.

### 3.3 Solid-state refrigeration

Solid-state refrigeration systems are excellent alternatives to vapor-compression refrigeration systems because they are convenient, energy-efficient, and environmentally friendly [121]. Solid-state refrigeration is based on the caloric effect of some refrigerant materials. When external fields (e.g., electrical fields) are applied, the temperature of these refrigerant materials will fluctuate, achieving the refrigerating objective. Figure 11 depicts a typical procedure for solid-state refrigeration systems. The heat flows in a cyclic process, from the heat source to the refrigerant material without an external field and then from the refrigerant material to the heat sink with an external field. In both the adiabatic and isothermal phases of the cycle, thermal switches and thermal regulators might restrict undesirable heat flow (e.g., heat flux from the heat sink to the refrigerant material), improving the energy efficiency and permitting a high energy density of the device.

In the electrocaloric refrigeration cycle, electrocaloric (EC) materials can cyclically work as thermal switches, making and breaking thermal contact between the hot source and the cold sink. Epstein et al. [122] applied thermal switch based on liquid crystal with  $r = 3.0$  in an EC cooling device. Some polymers can deform or translate when an electrical field is applied, accompanied by electrocaloric effects. On this basis, some researchers proposed thermal switches made of EC materials. Neese et al. [123] employed a ferroelectric [P(VDF-TrFE)] copolymer working as a thermal switch in the refrigeration cycle. Ma et al. [124] developed a P(VDF-TrFE-CFE) flexible polymer as a thermal switch that could adjust the thermal contact between the EC materials and the heat source/sink. This refrigeration system achieved a coefficient of performance (COP) of 13 and specific cooling power (SCP) of 2.8 W/g. Magnetocaloric solid-state refrigeration systems also attracted attention due to their potential to improve cooling efficiency. Silva et al. [125] theoretically investigated thermal switches made from a type of thermal smart material whose thermal resistance is controlled by a magnetic field. They discovered that the devices

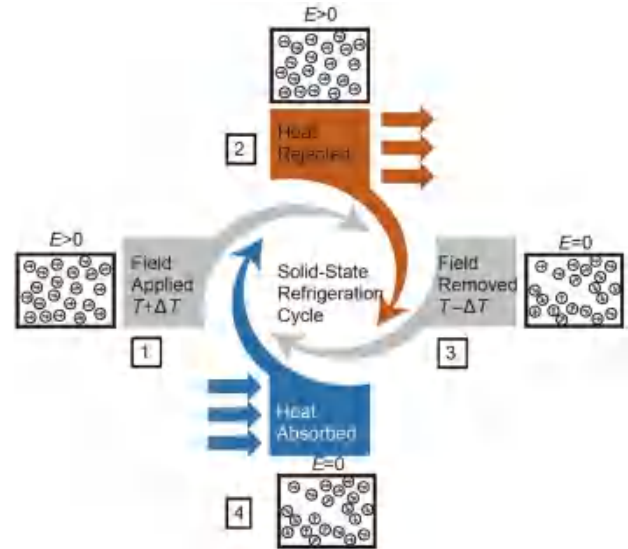


**Figure 11** (Color online) Thermodynamic solid-refrigeration cycle. The heat flows as a cyclic process. The cycle is composed of four processes. In the process 1→2, the applied external field increases the refrigerant material temperature  $T$  by  $\Delta T$ . During the process 2→3, heat flows from the refrigerant material to the heat sink. Removing the external field in the process 3→4 cools the refrigerant material, and in the process 4→1, heat flows from the heat source to the refrigerant material, achieving the refrigeration purpose [121].

could achieve a COP of 1.5 and an SCP of 2.75 W/cm<sup>2</sup> via a simulation method. Utaka et al. [126] proposed that a thermal switch with ferromagnetic material effectively improves the system performance, achieving a COP of 30.0.

### 3.4 Cryogenics

Cryogenics can provide the required operating environment for some high-sensitivity devices or weak signal measurements [127]. Adiabatic demagnetization refrigeration (ADR) is a typical cryogenic refrigeration technology based on the magnetocaloric effect [128]. Thermal switches, which can provide good thermal connection or isolation to the heat sink, are as essential in ADR as in room temperature refrigeration. Low temperature superconductors could work as thermal switches, with low thermal conductivity below the critical temperature and high thermal conductivity when a magnetic field is applied [129]. Table 6 shows several types of metals which can achieve a thermal switching ratio of  $r > 100$  when magnetic fields are kept below a critical temperature. Kruisius et al. [130] developed a superconductor thermal switch using Zn films with a thermal sensitivity of less than 50 mK. Furthermore, at very low temperatures, the magnetoresistive effects might cause the thermal conductivity of compensated metals to fluctuate by five orders of magnitude. To increase the performance of ADRs, Bartlett et al. [131] designed a tungsten magnetoresistive heat switch. The thermal switching ratio is  $r = 1.75 \times 10^4$  at  $T = 1.5$  K with  $B = 1.8$  T.

### 3.5 Thermal computers

Thermal switches and regulators are critical components in designing thermal logic gates. Theoretical designs are already available for most thermal logic gates, such as AND, OR, and NOT thermal logic gates. In thermal circuits, Boolean states can be defined as high and low temperature values,  $T_{\text{on}}$  and  $T_{\text{off}}$ , analogous to the “1” and “0” states in electric circuits. To achieve a thermal logic gate, a basic component that binarizes the input temperature is required. The component should output  $T_{\text{off}}$  ( $T_{\text{on}}$ ) if the input temperature is lower (higher) than the critical value  $T_c$  between  $T_{\text{off}}$  and  $T_{\text{on}}$ . Thermal switches [132] may be used to create these components. Considering the thermal switch in Figure 12(a), when the gate temperature  $T_G$  is near but not at  $T_{\text{off}}$  or  $T_{\text{on}}$ , the junction node temperature  $T_O$  will be closer to  $T_{\text{off}}$  or

$T_{\text{on}}$  owing to the heat flux in the device. When these thermal switches are connected in series, the final output will be very close to  $T_{\text{off}}$  or  $T_{\text{on}}$  precisely. Based on that, NOT, AND, and OR gates can all be implemented using this method. However, there are still certain theoretical and experimental obstacles to achieve these experimentally. Interfacial thermal resistance and heat leakage are inevitable problems in the connection of thermal devices. The theories offer limited accuracy for nanoscale interfacial resistance predictions, which makes the series structure not ideally work. Furthermore, the heat flux and thermal resistance of a single thermal device can no longer be precisely regulated to sufficiently realize logic functions. In addition to thermal logic gates, phononic computing requires thermal memory elements that can store information based on temperature. Xie et al. [55] suggested a viable solid-state thermal memory system based on the MIT of single-crystal  $\text{VO}_2$  nanobeams, as shown in Figure 12(b). The  $\text{VO}_2$  nanobeam could store and retain thermal information with two temperature states as input  $T_{\text{in}}$  and output  $T_{\text{out}}$  for reading and writing, achieving a nonlinear response in temperature. Applying voltage could improve the performance of these thermal memory elements. The element continued to work normally after over 150 cycles, proving its reliability.

**Table 6** Several superconductors as heat switches with magnetic field [127]

| Material | Critical transition temperature $T_c$ (K) | Critical magnetic field strength $B_c$ (mT) | Practical upper temperature $T_{\text{upper}}$ (K) |
|----------|---|---|--|
| Zn       | 0.85                                      | 5.3   | <0.1   |
| Al       | 1.2                                       | 10.5  | 0.1  |
| In       | 3.4                                       | 29.3  | 0.5  |
| Sn       | 3.7                                       | 30.9  | 0.52   |
| Pb       | 7.2                                       | 80.3  | 0.5  |

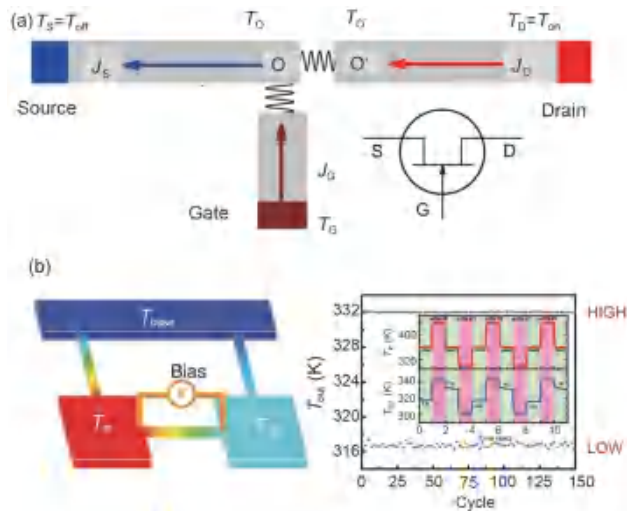


**Figure 12** (Color online) Thermal logic gate and thermal memory device. (a) Sketch of a thermal logic gate. It is composed of a source, a drain, and a gate. The temperatures in the source and drain are set as fixed values ( $T_D = T_{\text{off}}$ ,  $T_S = T_{\text{on}}$ ). As a thermal switch, the heat flux in the junction nodes O and O' can be controlled by adjusting  $T_G$  to different values [132]. (b) Experimental realization of the thermal memory element. Left is a schematic illustration of the thermal memory element. It is composed of an input terminal ( $T_{\text{in}}$ ), an output terminal ( $T_{\text{out}}$ ), and a conductive channel connecting the input and output terminals. The input and output terminals are connected to the substrate ( $T_{\text{base}}$ ). Right is the reversibility test. The inset presents the cycles of Write HIGH-Read-Write LOW-Read [55].

### 3.6 Thermal metamaterials

Metamaterials are artificial materials engineered to have unique properties compared to natural materials. The metamaterials are often constructed with a repetitive pattern, which distinguishes them from the original materials but makes their qualities reliant on the specified structures [133]. The anisotropy of their effective thermal conductivities can be engineered in a wide range by using composite structures. Because of their designed architectures, metamaterials could be used to explore physics mechanisms or be applied in industry. Manipulating waves, such as blocking, absorption, and enhancement, is possible by regulating the shape, size, and distribution of electromagnetic metamaterials [134]. As electromagnetic metamaterials advance, thermal metamaterials are also developing, and they are becoming an effective solution to control heat flux [135]. Fan et al. [136] developed a theoretical system of transformation thermology and used it to design thermal cloaking. As shown in Figure 13(a), a thermal cloak is characterized by a temperature gradient of zero in the central domain and an unaffected temperature field outside this domain, making it able to hide an object from detection by thermal observation outside the cloak. Narayana et al. [137] made the first manufactured thermal cloak made of multilayered composite experimentally, proving the transformation theory. Thermal cloaking may be expanded into switchable devices using thermal smart materials with temperature-dependent thermal con-

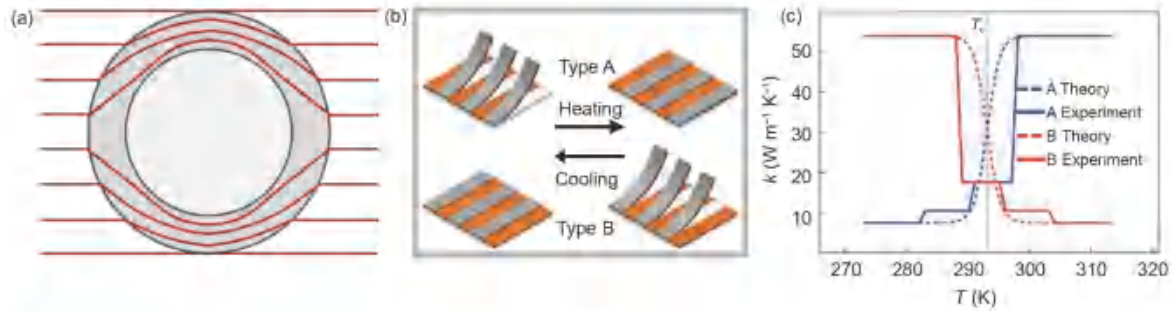


**Figure 13** (Color online) Thermal clock. (a) Sketch of the thermal clock. The red lines represent heat flow. (b) Schematic of two different types of materials [139]. (c) Thermal conductivity variation with temperature for these two types of materials [139].

ductivities. Li et al. [138] demonstrated temperature-dependent transformation thermology by introducing materials with tunable thermal conductivities. At the critical temperature threshold, the thermal conductivities of the base materials should change sharply, and phase change materials could be applied here. Shen et al. [139] proposed a thermal resistor made of phosphor copper and shape memory alloy (SMA) that functions as a thermal smart material. Using two types of SMAs, when the ambient temperature changes, the temperature in the central domain can be stabilized (Figure 13(b)). In addition to thermal cloaking, thermal concentrating also attracts attention because it increases the central heat flux without affecting the outside temperature distribution and helps harvest heat energy. Li et al. [140] proposed a flexible and switchable thermal concentrating device made of phase change materials. In addition, thermal convection is an effective method to modify the heat transfer in moving matter. In forced thermal convection where the background material is in motion, the velocity of the background material is a continuously tunable parameter that could modify the heat transfer directly, leading to the variation of effective thermal conductivity. Li et al. [141] proposed a mechanically rotating system that mimics a solid-like material whose thermal conductivity dynamically covers a wide range. It can achieve the effects of thermal zero-index cloaking. Xu et al. [142] reported an analog thermal material whose effective conductivity can be tuned from near-zero to near-infinity thermal conductivity via thermal convection.

#### 4 Summary and outlook

Although research on thermal smart materials has gone through several years, it is still in the preliminary stage. Recently, the materials and excitation methods have become diversified and easily manipulated, which is more suitable for practical applications. Thermal smart components and devices based on thermal smart materials indicate a new frontier, which can allow more active and effective thermal control, improve thermal management performance and even

inspire new techniques, such as thermal computers. The thermal switching ratio of available thermal smart materials has been gradually increasing and can reach near  $r = 10$  in the laboratory now. However, most studies still fail to industrialize. One important reason is that their characteristic performances are flawed. For example, using electrochemical methods to tune the thermal conductivity of layered materials, the response time is at least on the order of minutes, not adapting to the needs of fast adjustment. Although polymers have good responses to external fields, their thermal conductivity is quite poor, reducing their application value. To go further in this field, thermal smart materials should perform much better than in current studies. Furthermore, current studies mainly focus on the thermal switching ratio, but other performance parameters, such as recyclability, response time, the absolute value of thermal conductance, and economic efficiency, all play key roles.

In the future, nanomaterials with excellent thermal properties, such as carbon nanotubes or graphene, could make more contributions to this field. Nanoscale thermal smart materials can be used for small-scale heat control, such as microelectronic device thermal management. Meanwhile, thermal smart materials should be enlarged to integrate and operate in other situations. Macro-scale thermal smart components could be used in solid-state refrigeration to control heat flux in thermal circuits. In addition to adapting to various multiscale systems, devices based on thermal smart materials must function properly in different thermal environments, such as extremely high or low temperatures, placing higher requirements on the stability of materials. This need will motivate fundamental research into new solid-state materials, such as solid-solid phase change materials. The “carbon neutrality” goal imposed more pressing demands for thermal smart materials in the energy sector. To make progress in the development of thermal smart materials, it is necessary to develop corresponding theories for preparing thermal smart materials with improved performance, including the effects of applied fields on the microstructure of materials and heat conduction mechanisms at both the macro and microscale. In addition, advanced ex-

perimental technologies are also necessary. There is still a long way to go in the field of thermal smart materials and their applications. Exploring new types of thermal smart materials, achieving a larger switching ratio and comprehensive performance, and inventing new thermal smart devices are still the most important challenges in the future.

*The work was supported by the National Natural Science Foundation of China (Grant Nos. 51825601, and U20A20301).*

- 1 A. L. Moore, and L. Shi, *Mater. Today* **17**, 163 (2014).
- 2 D. Hengeveld, M. Mathison, J. Braun, E. Groll, and A. Williams, *HVAC&R Res.* **16**, 189 (2010).
- 3 G. Wehmeyer, T. Yabuki, C. Monachon, J. Wu, and C. Dames, *Appl. Phys. Rev.* **4**, 041304 (2017).
- 4 H. Zhang, F. X. Che, T. Y. Lin, and W. Zhao, *Modeling, Analysis, Design, and Tests for Electronics Packaging Beyond Moore* (Woodhead Publishing, London, 2019), pp. 1-12.
- 5 K. Klinar, T. Swoboda, M. Muñoz Rojo, and A. Kitanovski, *Adv. Electron. Mater.* **7**, 2000623 (2021).
- 6 Q. An, B. Zhang, X. Zhou, C. Li, J. Wang, and L. Wang, *Heat Mass Transfer* **56**, 1077 (2020).
- 7 Z. Q. Hou, and J. G. Hu, *Thermal Control Technology of Spacecraft* (Science and Technology of China Press, Beijing, 2007), pp. 1-11.
- 8 M. T. F. Rodrigues, G. Babu, H. Gullapalli, K. Kalaga, F. N. Sayed, K. Kato, J. Joyner, and P. M. Ajayan, *Nat. Energy* **2**, 17108 (2017).
- 9 R. Prasher, *Proc. IEEE* **94**, 1571 (2006).
- 10 B. Esser, J. Barcena, M. Kuhn, A. Okan, L. Haynes, S. Gianella, A. Ortona, V. Liedtke, D. Francesconi, and H. Tanno, *J. Spacecraft Rockets* **53**, 1051 (2016).
- 11 J. Wang, Y. Li, X. Liu, C. Shen, H. Zhang, and K. Xiong, *Chin. J. Aeronaut.* **34**, 1 (2021).
- 12 C. W. Chang, D. Okawa, A. Majumdar, and A. Zettl, *Science* **314**, 1121 (2006).
- 13 T. Swoboda, K. Klinar, A. S. Yalamarthy, A. Kitanovski, and M. M. Rojo, *Adv. Electron. Mater.* **7**, 2000625 (2021).
- 14 R. H. Baughman, A. A. Zakhidov, and W. A. de Heer, *Science* **297**, 787 (2002).
- 15 A. K. Geim, *Science* **324**, 1530 (2009), arXiv: 0906.3799.
- 16 C. Kleinstreuer, and Y. Feng, *Nanoscale Res. Lett.* **6**, 439 (2011).
- 17 S. Pil Jang, and S. U. S. Choi, *J. Heat Transfer* **129**, 617 (2007).
- 18 Y. Xu, X. Wang, and Q. Hao, *Compos. Commun.* **24**, 100617 (2021).
- 19 A. I. Oliva-Avilés, F. Avilés, V. Sosa, A. I. Oliva, and F. Gamboa, *Nanotechnology* **23**, 465710 (2012).
- 20 G. Korneva, H. Ye, Y. Gogotsi, D. Halverson, G. Friedman, J. C. Bradley, and K. G. Kornev, *Nano Lett.* **5**, 879 (2005).
- 21 E. K. Hobbie, H. Wang, H. Kim, S. Lin-Gibson, and E. A. Grulke, *Phys. Fluids* **15**, 1196 (2003).
- 22 D. J. Dijkstra, M. Cirstea, and N. Nakamura, *Rheol. Acta* **49**, 769 (2010).
- 23 N. Song, D. Jiao, P. Ding, S. Cui, S. Tang, and L. Shi, *J. Mater. Chem. C* **4**, 305 (2016).
- 24 A. M. Marconnet, N. Yamamoto, M. A. Panzer, B. L. Wardle, and K. E. Goodson, *ACS Nano* **5**, 4818 (2011).
- 25 B. Y. Cao, and R. Y. Dong, *J. Chem. Phys.* **140**, 034703 (2014).
- 26 R. Y. Dong, and B. Y. Cao, *Sci. Rep.* **4**, 6120 (2014).
- 27 R. Y. Dong, P. Cao, G. X. Cao, G. J. Hu, and B. Y. Cao, *Acta Phys. Sin.* **66**, 014702 (2017).
- 28 M. Monti, M. Natali, L. Torre, and J. M. Kenny, *Carbon* **50**, 2453 (2012).
- 29 C. W. Nan, R. Birringer, D. R. Clarke, and H. Gleiter, *J. Appl. Phys.* **81**, 6692 (1997).
- 30 R. Prasher, W. Evans, P. Meakin, J. Fish, P. Phelan, and P. Keblinski, *Appl. Phys. Lett.* **89**, 143119 (2006).
- 31 Z. T. Zhang, R. Y. Dong, D. S. Qiao, and B. Y. Cao, *Nanotechnology* **31**, 465403 (2020).
- 32 J. Philip, P. D. Shima, and B. Raj, *Appl. Phys. Lett.* **91**, 203108 (2007).
- 33 J. Philip, P. D. Shima, and B. Raj, *Appl. Phys. Lett.* **92**, 043108 (2008).
- 34 P. D. Shima, J. Philip, and B. Raj, *Appl. Phys. Lett.* **95**, 133112 (2009).
- 35 C. L. Altan, A. Elkatmis, M. Yüksel, N. Aslan, and S. Bucak, *J. Appl. Phys.* **110**, 093917 (2011).
- 36 P. C. Sun, Y. Huang, R. T. Zheng, G. A. Cheng, Q. M. Wan, and Y. L. Ding, *Mater. Lett.* **149**, 92 (2015).
- 37 B. Abeles, *Phys. Rev.* **131**, 1906 (1963).
- 38 G. Zhu, J. Liu, Q. Zheng, R. Zhang, D. Li, D. Banerjee, and D. G. Cahill, *Nat. Commun.* **7**, 13211 (2016).
- 39 X. Qian, X. Gu, M. S. Dresselhaus, and R. Yang, *J. Phys. Chem. Lett.* **7**, 4744 (2016).
- 40 N. Lu, P. Zhang, Q. Zhang, R. Qiao, Q. He, H. B. Li, Y. Wang, J. Guo, D. Zhang, Z. Duan, Z. Li, M. Wang, S. Yang, M. Yan, E. Arenholz, S. Zhou, W. Yang, L. Gu, C. W. Nan, J. Wu, Y. Tokura, and P. Yu, *Nature* **546**, 124 (2017).
- 41 J. Cho, M. D. Losego, H. G. Zhang, H. Kim, J. Zuo, I. Petrov, D. G. Cahill, and P. V. Braun, *Nat. Commun.* **5**, 4035 (2014).
- 42 J. N. Reimers, and J. R. Dahn, *J. Electrochem. Soc.* **139**, 2091 (1992).
- 43 J. S. Kang, M. Ke, and Y. Hu, *Nano Lett.* **17**, 1431 (2017).
- 44 J. Sun, H. W. Lee, M. Pasta, H. Yuan, G. Zheng, Y. Sun, Y. Li, and Y. Cui, *Nat. Nanotech.* **10**, 980 (2015).
- 45 A. Sood, F. Xiong, S. Chen, H. Wang, D. Selli, J. Zhang, C. J. McClellan, J. Sun, D. Donadio, Y. Cui, E. Pop, and K. E. Goodson, *Nat. Commun.* **9**, 4510 (2018), arXiv: 1901.04639.
- 46 T. Tadano, Y. Gohda, and S. Tsuneyuki, *Phys. Rev. Lett.* **114**, 095501 (2015), arXiv: 1412.5723.
- 47 Q. Lu, S. Huberman, H. Zhang, Q. Song, J. Wang, G. Vardar, A. Hunt, I. Waluyo, G. Chen, and B. Yildiz, *Nat. Mater.* **19**, 655 (2020).
- 48 E. S. Toberer, L. L. Baranowski, and C. Dames, *Annu. Rev. Mater. Res.* **42**, 179 (2012).
- 49 S. R. Bishop, D. Marrocchelli, C. Chatzichristodoulou, N. H. Perry, M. B. Mogenssen, H. L. Tuller, and E. D. Wachsman, *Annu. Rev. Mater. Res.* **44**, 205 (2014).
- 50 H. Nazir, M. Batool, F. J. Bolivar Osorio, M. Isaza-Ruiz, X. Xu, K. Vignarooban, P. Phelan, P. Inamuddin, and A. M. Kannan, *Int. J. Heat Mass Transfer* **129**, 491 (2019).
- 51 A. Sharma, A. Shukla, C. R. Chen, and T. N. Wu, *Sust. Energy Tech. Assess.* **7**, 17 (2014).
- 52 A. Fiorino, D. Thompson, L. Zhu, R. Mittapally, S. A. Biehs, O. Bezenecet, N. El-Bondry, S. Bansropun, P. Ben-Abdallah, E. Meyhofer, and P. Reddy, *ACS Nano* **12**, 5774 (2018).
- 53 C. N. Berglund, and H. J. Guggenheim, *Phys. Rev.* **185**, 1022 (1969).
- 54 V. N. Andreev, F. A. Chudnovskii, A. V. Petrov, and E. I. Terukov, *Phys. Stat. Sol. A* **48**, K153 (1978).
- 55 R. Xie, C. T. Bui, B. Varghese, Q. Zhang, C. H. Sow, B. Li, and J. T. L. Thong, *Adv. Funct. Mater.* **21**, 1602 (2011).
- 56 K. Dahal, Q. Zhang, Y. Wang, I. K. Mishra, and Z. Ren, *RSC Adv.* **7**, 33775 (2017).
- 57 H. Kizuka, T. Yagi, J. Jia, Y. Yamashita, S. Nakamura, N. Taketoshi, and Y. Shigesato, *Jpn. J. Appl. Phys.* **54**, 053201 (2015).
- 58 D. W. Oh, C. Ko, S. Ramanathan, and D. G. Cahill, *Appl. Phys. Lett.* **96**, 151906 (2010).
- 59 S. Lee, K. Hippalgaonkar, F. Yang, J. Hong, C. Ko, J. Suh, K. Liu, K. Wang, J. J. Urban, X. Zhang, C. Dames, S. A. Hartnoll, O. Delaire, and J. Wu, *Science* **355**, 371 (2017).
- 60 A. Ayuela, J. Enkovaara, K. Ullakko, and R. M. Nieminen, *J. Phys.-Condens. Matter* **11**, 2017 (1999).
- 61 V. D. Buchel'nikov, A. N. Vasiliev, V. V. Koledov, S. V. Taskaev, V. V. Khovaylo, and V. G. Shavrov, *Phys. Usp.* **49**, 871 (2006).
- 62 A. B. Batdalov, A. M. Aliev, L. N. Khanov, V. D. Buchel'nikov, V.

- V. Sokolovskii, V. V. Koledov, V. G. Shavrov, A. V. Mashirov, and E. T. Dil'mieva, *J. Exp. Theor. Phys.* **122**, 874 (2016).
- 63 Q. Zheng, S. E. Murray, Z. Diao, A. Bhutani, D. P. Shoemaker, and D. G. Cahill, *Phys. Rev. Mater.* **2**, 075401 (2018).
- 64 Q. Zheng, G. Zhu, Z. Diao, D. Banerjee, and D. G. Cahill, *Adv. Eng. Mater.* **21**, 1801342 (2019).
- 65 M. Wuttig, and N. Yamada, *Nat. Mater.* **6**, 824 (2007).
- 66 L. Yang, and B. Y. Cao, *J. Phys. D-Appl. Phys.* **54**, 505302 (2021).
- 67 E. Bozorg-Grayeli, J. P. Reifenberg, M. Asheghi, H. S. P. Wong, and K. E. Goodson, *Annu. Rev. Heat Transfer* **16**, 397 (2013).
- 68 H. K. Lyee, D. G. Cahill, B. S. Lee, J. R. Abelson, M. H. Kwon, K. B. Kim, S. G. Bishop, and B. Cheong, *Appl. Phys. Lett.* **89**, 151904 (2006).
- 69 J. P. Reifenberg, M. A. Panzer, S. B. Kim, A. M. Gibby, Y. Zhang, S. Wong, H. S. P. Wong, E. Pop, and K. E. Goodson, *Appl. Phys. Lett.* **91**, 111904 (2007).
- 70 K. Ghosh, A. Kusiak, P. Noé, M. C. Cyrille, and J. L. Battaglia, *Phys. Rev. B* **101**, 214305 (2020), arXiv: 2006.02625.
- 71 R. Zheng, J. Gao, J. Wang, and G. Chen, *Nat. Commun.* **2**, 289 (2011).
- 72 S. A. Angayarkanni, and J. Philip, *J. Phys. Chem. C* **118**, 13972 (2014).
- 73 S. A. Angayarkanni, and J. Philip, *J. Appl. Phys.* **118**, 094306 (2015).
- 74 S. Harish, K. Ishikawa, S. Chiashi, J. Shiomi, and S. Maruyama, *J. Phys. Chem. C* **117**, 15409 (2013).
- 75 P. C. Sun, Y. L. Wu, J. W. Gao, G. A. Cheng, G. Chen, and R. T. Zheng, *Adv. Mater.* **25**, 4938 (2013).
- 76 R. J. Warzoha, R. M. Weigand, and A. S. Fleischer, *Appl. Energy* **137**, 716 (2015).
- 77 Y. Wu, X. Yan, P. Meng, P. Sun, G. Cheng, and R. Zheng, *Carbon* **94**, 417 (2015).
- 78 H. A. Barnes, *Chem. Eng. J.* **79**, 84 (2000).
- 79 H. Hu, M. Gopinadhan, and C. O. Osuji, *Soft Matter* **10**, 3867 (2014).
- 80 J. Shin, J. Sung, M. Kang, X. Xie, B. Lee, K. M. Lee, T. J. White, C. Leal, N. R. Sottos, P. V. Braun, and D. G. Cahill, *Proc. Natl. Acad. Sci.* **116**, 5973 (2019).
- 81 C. Li, Y. Ma, and Z. Tian, *ACS Macro Lett.* **7**, 53 (2018).
- 82 R. Shrestha, Y. Luan, S. Shin, T. Zhang, X. Luo, J. S. Lundh, W. Gong, M. R. Bockstaller, S. Choi, T. Luo, R. Chen, K. Hippalgaonkar, and S. Shen, *Sci. Adv.* **5**, eaax3777 (2019).
- 83 T. Zhang, and T. Luo, *ACS Nano* **7**, 7592 (2013).
- 84 J. A. Tomko, A. Pena-Francesch, H. Jung, M. Tyagi, B. D. Allen, M. C. Demirel, and P. E. Hopkins, *Nat. Nanotech.* **13**, 959 (2018).
- 85 J. Shin, M. Kang, T. Tsai, C. Leal, P. V. Braun, and D. G. Cahill, *ACS Macro Lett.* **5**, 955 (2016).
- 86 C. Liu, Y. Chen, and C. Dames, *Phys. Rev. Appl.* **11**, 044002 (2019).
- 87 P. E. Hopkins, C. Adamo, L. Ye, B. D. Huey, S. R. Lee, D. G. Schlom, and J. F. Ihlefeld, *Appl. Phys. Lett.* **102**, 121903 (2013).
- 88 B. M. Foley, M. Wallace, J. T. Gaskins, E. A. Paisley, R. L. Johnson-Wilke, J. W. Kim, P. J. Ryan, S. Trolrier-McKinstry, P. E. Hopkins, and J. F. Ihlefeld, *ACS Appl. Mater. Interfaces* **10**, 25493 (2018).
- 89 J. F. Ihlefeld, B. M. Foley, D. A. Scrymgeour, J. R. Michael, B. B. McKenzie, D. L. Medlin, M. Wallace, S. Trolrier-McKinstry, and P. E. Hopkins, *Nano Lett.* **15**, 1791 (2015).
- 90 S. Yiğen, and A. R. Champagne, *Nano Lett.* **14**, 289 (2014), arXiv: 1401.3030.
- 91 K. N. Kalaidjiev, M. P. Mikhailov, G. I. Bozhanov, and S. R. Stoyanov, *Phys. Stat. Sol. A* **69**, K163 (1982).
- 92 S. Deng, J. Yuan, Y. Lin, X. Yu, D. Ma, Y. Huang, R. Ji, G. Zhang, and N. Yang, *Nano Energy* **82**, 105749 (2021).
- 93 S. Deng, D. Ma, G. Zhang, and N. Yang, *J. Mater. Chem. A* **9**, 24472 (2021).
- 94 J. Kimling, K. Nielsch, K. Rott, and G. Reiss, *Phys. Rev. B* **87**, 497 (2013).
- 95 J. M. Ziman, *Electrons and Phonons* (Oxford University Press, Britain, 1960), pp. 1-20.
- 96 F. Y. Yang, K. Liu, K. Hong, D. H. Reich, P. C. Searson, and C. L. Chien, *Science* **284**, 1335 (1999).
- 97 M. N. Baibich, J. M. Broto, A. Fert, F. N. Van Dau, F. Petroff, P. Etienne, G. Creuzet, A. Friederich, and J. Chazelas, *Phys. Rev. Lett.* **61**, 2472 (1988).
- 98 J. Kimling, R. B. Wilson, K. Rott, J. Kimling, G. Reiss, and D. G. Cahill, *Phys. Rev. B* **91**, 144405 (2015).
- 99 R. Jin, Y. Onose, Y. Tokura, D. Mandrus, P. Dai, and B. C. Sales, *Phys. Rev. Lett.* **91**, 146601 (2003).
- 100 S. Dhara, H. S. Solanki, R. Arvind Pawan, V. Singh, S. Sengupta, B. A. Chalke, A. Dhar, M. Gokhale, A. Bhattacharya, and M. M. Deshmukh, *Phys. Rev. B* **84**, 121307 (2011), arXiv: 1106.2880.
- 101 H. T. Huang, M. F. Lai, Y. F. Hou, and Z. H. Wei, *Nano Lett.* **15**, 2773 (2015).
- 102 X. Zhao, J. C. Wu, Z. Y. Zhao, Z. Z. He, J. D. Song, J. Y. Zhao, X. G. Liu, X. F. Sun, and X. G. Li, *Appl. Phys. Lett.* **108**, 242405 (2016), arXiv: 1606.02010.
- 103 C. McGuire, K. Sawchuk, and A. Kavner, *J. Appl. Phys.* **124**, 115902 (2018).
- 104 A. V. Talyzin, O. Andersson, B. Sundqvist, A. Kurnosov, and L. Dubrovinsky, *J. Solid State Chem.* **180**, 510 (2007).
- 105 X. B. Li, K. Maute, M. L. Dunn, and R. G. Yang, *Phys. Rev. B* **81**, 285 (2010).
- 106 H. Meng, D. Ma, X. Yu, L. Zhang, Z. Sun, and N. Yang, *Int. J. Heat Mass Transfer* **145**, 118719 (2019).
- 107 H. Meng, S. Maruyama, R. Xiang, and N. Yang, *Int. J. Heat Mass Transfer* **180**, 121773 (2021).
- 108 S. Li, X. Yu, H. Bao, and N. Yang, *J. Phys. Chem. C* **122**, 13140 (2018).
- 109 X. Wan, B. Demir, M. An, T. R. Walsh, and N. Yang, *Int. J. Heat Mass Transfer* **180**, 121821 (2021).
- 110 Y. Zeng, C. L. Lo, S. Zhang, Z. Chen, and A. Marconnet, *Carbon* **158**, 63 (2020).
- 111 T. Du, Z. Xiong, L. Delgado, W. Liao, J. Peoples, R. Kantharaj, P. R. Chowdhury, A. Marconnet, and X. Ruan, *Nat. Commun.* **12**, 4915 (2021).
- 112 D. Yu, Y. Liao, Y. Song, S. Wang, H. Wan, Y. Zeng, T. Yin, W. Yang, and Z. He, *Adv. Sci.* **7**, 2000177 (2020).
- 113 Y. Yang, and W. Gao, *Chem. Soc. Rev.* **48**, 1465 (2019).
- 114 Q. Song, M. An, X. Chen, Z. Peng, J. Zang, and N. Yang, *Nanoscale* **8**, 14943 (2016).
- 115 N. Yang, X. Ni, J. W. Jiang, and B. Li, *Appl. Phys. Lett.* **100**, 093107 (2012), arXiv: 1207.0285.
- 116 B. Y. Cao, and D. S. Qiao, *Thermal Resistor*, China Patent, ZL201810298324.6 (2020-04-24).
- 117 G. J. Hu, G. X. Cao, D. S. Qiao, and B. Y. Cao, *J. Eng. Thermophys.* **40**, 1380 (2019).
- 118 A. Henry, R. Prasher, and A. Majumdar, *Nat. Energy* **5**, 635 (2020).
- 119 K. Menyhart, and M. Krarti, *Build. Environ.* **114**, 203 (2017).
- 120 S. J. M. Koenders, R. C. G. M. Loonen, and J. L. M. Hensen, *Energy Build.* **173**, 409 (2018).
- 121 K. Klinar, and A. Kitanovski, *Renew. Sustain. Energy Rev.* **118**, 109571 (2020).
- 122 R. I. Epstein, and K. J. Malloy, *J. Appl. Phys.* **106**, 064509 (2009).
- 123 B. Neese, B. Chu, S. G. Lu, Y. Wang, E. Furman, and Q. M. Zhang, *Science* **321**, 821 (2008).
- 124 R. Ma, Z. Zhang, K. Tong, D. Huber, R. Kornbluh, Y. S. Ju, and Q. Pei, *Science* **357**, 1130 (2017).
- 125 D. J. Silva, B. D. Bordalo, A. M. Pereira, J. Ventura, and J. P. Araújo, *Appl. Energy* **93**, 570 (2012).
- 126 Y. Utaka, K. Hu, Z. Chen, and Y. Zhao, *Appl. Thermal Eng.* **155**, 196 (2019).
- 127 Q. Shu, J. Demko, and J. Fesmire, in *IOP Conference Series: Materials Science and Engineering*, edited by J. G. Weisend II (IOP Publishing, Wisconsin, 2017), p. 012133.
- 128 M. J. DiPirro, and P. J. Shirron, *Cryogenics* **62**, 172 (2014).
- 129 V. P. Peshkov, and A. Y. Parshin, *Sov. Phys. JETP* **21**, 258 (1965).

- 130 M. Krusius, D. N. Paulson, and J. C. Wheatley, *Rev. Sci. Instrum.* **49**, 396 (1978).
- 131 J. Bartlett, G. Hardy, I. Hepburn, R. Ray, and S. Weatherstone, *Cryogenics* **50**, 647 (2010).
- 132 N. Li, J. Ren, L. Wang, G. Zhang, P. Hänggi, and B. Li, *Rev. Mod. Phys.* **84**, 1045 (2012), arXiv: [1108.6120](https://arxiv.org/abs/1108.6120).
- 133 Y. Li, W. Li, T. Han, X. Zheng, J. Li, B. Li, S. Fan, and C. W. Qiu, *Nat. Rev. Mater.* **6**, 488 (2021), arXiv: [2008.07964](https://arxiv.org/abs/2008.07964).
- 134 D. Schurig, J. J. Mock, B. J. Justice, S. A. Cummer, J. B. Pendry, A. F. Starr, and D. R. Smith, *Science* **314**, 977 (2006).
- 135 S. Yang, J. Wang, G. Dai, F. Yang, and J. Huang, *Phys. Rep.* **908**, 1 (2021).
- 136 C. Z. Fan, Y. Gao, and J. P. Huang, *Appl. Phys. Lett.* **92**, 251907 (2008).
- 137 S. Narayana, and Y. Sato, *Phys. Rev. Lett.* **108**, 214303 (2012).
- 138 Y. Li, X. Shen, Z. Wu, J. Huang, Y. Chen, Y. Ni, and J. Huang, *Phys. Rev. Lett.* **115**, 195503 (2015), arXiv: [1505.00971](https://arxiv.org/abs/1505.00971).
- 139 X. Shen, Y. Li, C. Jiang, and J. Huang, *Phys. Rev. Lett.* **117**, 055501 (2016).
- 140 Y. Li, X. Shen, J. Huang, and Y. Ni, *Phys. Lett. A* **380**, 1641 (2016).
- 141 J. Li, Y. Li, P. C. Cao, T. Yang, X. F. Zhu, W. Wang, and C. W. Qiu, *Adv. Mater.* **32**, 2003823 (2020).
- 142 G. Xu, K. Dong, Y. Li, H. Li, K. Liu, L. Li, J. Wu, and C. W. Qiu, *Nat. Commun.* **11**, 6028 (2020).